Journal of Agriculture and Food Research 14 (2023) 100759

Contents lists available at ScienceDirect

Journal of Agriculture and Food Research

journal homepage: www.sciencedirect.com/journal/journal-of-agriculture-and-food-research

Development of nanocomposite chitosan films with antimicrobial activity from agave bagasse and shrimp shells

Gabriela Montes de Oca-Vásquez [a], Marianelly Esquivel-Alfaro [b], José Roberto Vega-Baudrit [a,b], Guillermo Jiménez-Villalta [b], Víctor Hugo Romero-Arellano [c], Belkis Sulbarán-Rangel [c,*]

[a] National Nanotechnology Laboratory (LANOTEC), National Center for High Technology, 10109, Pavas, San José, Costa Rica
[b] Laboratory of Polymer Science and Technology (POLIUNA), School of Chemistry, Universidad Nacional, Campus Omar Dengo, 40101, Heredia, Costa Rica
[c] Department of Water and Energy, University of Guadalajara, Campus Tonalá, Tonalá, 45425, Mexico

ARTICLE INFO

Keywords:
Nanocellulose
Silver nanoparticles
Chitosan
Packaging
Antimicrobial

ABSTRACT

In this study, the nanocomposite chitosan films with antimicrobial activity from agave bagasse and shrimp shells were developed. Chitosan was successfully extracted from shrimp shells waste and cellulose nanofibers were obtained from bagasse agave. To improve the antimicrobial activity, different silver nanoparticle concentrations (2.5, 5, and 10% v/v) were added in the formulation. The films were prepared using the solvent casting technique and the film samples were characterized by Fourier transform infrared spectroscopy, thermogravimetric analysis, and scanning electron microscopy. The functional properties were also evaluated, including transparency, antibacterial activity (against *Escherichia coli)*, water-solubility, swelling, and mechanical properties. The moisture content and water solubility decreased when the silver nanoparticles and nanofiber were added to the films. An increase in strength and modulus was determined when the nanofibers were added to the film. and with the addition of silver nanoparticles a decrease of the mechanical properties proportional to the nanoparticle content was observed. Therefore, there was an increase in the mechanical properties of chitin films with the incorporation of nanofibers and the addition of 2.5% and 5% of silver nanoparticles. Chitosan/nanofiber-based films displayed a total antibacterial activity against *E.coli* compared to chitosan-based films, with a synergistic effect between chitosan and cellulose nanofibers. This work highlights the potential of chitosan films reinforced with nanofibers and silver nanoparticles to act as green alternative for food preservation and packaging.

1. Introduction

Nowadays, there has been a great need to substitute petroleum-derived packaging materials due to their non-biodegradable nature and the limitation of petrochemical resources [1,2]. To replace fossil-derived synthetic polymers and to minimize the problem of the accumulation of plastics in the environment, biopolymers have received great attention due to their remarkably reduced dependence on petroleum and for being environmental-friendly and biodegradable properties [3,4]. Chitosan (CHT) has emerged as an attractive material for the food packaging industry due to its excellent properties [3,5,6], abundance, non-toxic, biodegradable, barrier, antibacterial and film-forming properties [3,7]. CHT is prepared by the deacetylation of chitin, the second most abundant biopolymer after cellulose on Earth [8,9]. Chitin polymer can be found in the exoskeletons of arthropods (e.g., shrimps, lobsters, and crabs), as well as in fungi and yeast cell walls [3]. Structurally, chitin is a linear amino polysaccharide with variable molecular weight, with D-glucosamine and N-acetyl-D-glucosamine units bonded by β-1,4 glycosidic linkages [8,10,11].

Nevertheless, the production of CHT films is a challenge mainly because of their high water-solubility, and low structural and mechanical properties [5]. These limitations could be improved by using different approaches, e.g plasticizers, cross-linkers and emulsifiers, fibers, nanoparticles, natural extracts, essential oils and CHT blend films with polysaccharides, proteins, and synthetic polymers [9]. Glycerol is a plasticizer frequently added to increase the mobility between the polymer molecular chains and then reducing their intermolecular forces [12]. Nanocellulose (NC), either as nanocrystals (CNC), nanofibers (CNF) or cellulose nanoparticles (CNP) form, has been widely used as a reinforcing material to improve the mechanical, structural, and thermal properties of CHT films [13–16]. Agricultural residues are abundant and represent an alternative to obtain added-value products, such as

* Corresponding author.
E-mail address: belkis.sulbaran@academicos.udg.mx (B. Sulbarán-Rangel).

https://doi.org/10.1016/j.jafr.2023.100759
Received 20 May 2023; Received in revised form 22 August 2023; Accepted 24 August 2023
Available online 25 August 2023

nanocellulose. The advantage of using these lignocellulosic materials is that they are normally by-products from industrial processes or agricultural activities; they are available in large quantities and are an economic source [17]. Agave bagasse is an abundant source of biomass, very relevant to the state of Jalisco, Mexico, because it is a waste of the tequila industry, which is derived from *Agave tequilana* plant [18]. Some studies have used agave bagasse to obtain CNC and CNF [18–21], which is an excellent strategy due to the abundance of this agricultural residue.

Besides mechanical, structural, and thermal properties, antimicrobial activity is another important characteristic of active films. The addition of nanoparticles (NPs) such as TiO_2NPs [22,23], ZnONPs [24,25], CuNPs [26], and silver nanoparticles (AgNPs) [11,14,27,28], can enhance the antimicrobial capacity of the CHT film. Among these NPs, AgNPs have recently been used in food preservation for their excellent antibacterial and antifungal ability [26,29]. Different studies have shown, that when applied to CHT films, AgNPs can improve the mechanical, optical, thermal stability, and antimicrobial activity [7]. Despite some studies reporting the combination of CHT with CNF and/or AgNPs for food packaging applications [15,30], literature concerning the use of cellulose nanofiber from agave fibers in the food packaging industry is scarce. Furthermore, studies are focused mainly on the development of nanocomposites based on cornstarch and cellulose nanofibrils from *Agave tequilana* Weber [21]. Therefore, the present study is mainly focused on producing chitosan films reinforced with CNF, obtained from bagasse agave fibers, and AgNPs, synthesized by a sonochemical method, using chitosan extracted from shrimp exoskeleton as a stabilizing agent. The aim of this study is to develope a flexible, transparent, resistant composite material with antibacterial properties to be used as packaging and in the preservation of food, in addition to giving added value to little used waste such as shrimp shells and agave bagasse.

2. Materials and methods

2.1. Materials

The Laboratory of Polymer Science and Technology (POLIUNA) in Costa Rica provided the chitosan, which is obtained from shrimp shells residue. The bagasse fibers of the *Agave Tequilana Weber* plant was sourced from a tequila company in Tlajomulco de Zúñiga Jalisco, Mexico. Pure acetic acid and glycerol (99 wt% purity) were obtained from Merck Co., Germany. Nutrient Broth and Nutrient Agar were purchased from Becton, Dickinson and Company, Sparks, MD, USA. American Type Culture Collection, USA, supplied *Escherichia coli 25922*. The chemical reagents used included hydrochloric acid (HCl), sodium hydroxide (NaOH), and sodium acetate (CH_3COONa) which were acquired from Sigma-Aldrich.

2.2. Preparation and characterization of chitosan

During a preliminary stage to extract the chitin, shrimp shells as a by-product of an aquaculture process were obtained from a company located in the Pacific coast of Costa Rica. Subsequently, the material was milled and subjected to a treatment with hydrochloric acid 5% w/w and then sodium hydroxide 5% w/w, at room temperature. Afterwards, the material was washed until neutral pH was reached and dried in a solar oven. In order to obtain chitosan, deacetylation of chitin was carried out using 50% w/w NaOH at 100 °C for 2 h with constant stirring at 200 rpm. Once the reaction time had elapsed, the mixture was filtered and washed until reaching neutral pH. Finally, the chitosan was dried in an oven at 70 °C. The chitosan was characterized by determining its molecular weight, using a viscosimetric technique; a buffer of 0.25 M acetic acid/0.25 M sodium acetate was used and the Mark–Houwink–Sakurada constants of $K = 1.57 \times 10^{-4}$ and $a = 0.79$ were used to estimate the viscosimetric molecular weight (Mv) [31]. The deacetylation degree of the material was assessed by a conductometric titration using HCl 0.1 M as solvent and NaOH 0.1 M as titrant [32]. The material extracted had a molecular weight of 420 kDa and a deacetylation degree of 73%.

2.3. Isolation and characterization of nanofibrillar cellulose

Cellulose nanofibers (CNF) were obtained from cellulose bagasse agave. Cellulose was isolated via organosolv treatment and bleached according to previous work [18,33]. CNF was produced by mechanical microfluidization (Microfluidizer M − 110P, United States) with a pressure range of 2000 to 30,000 psi. Agave cellulose with a consistency of 1.5% is passed several times through the microfluidizer using the 400 and 200 μm chambers arranged in series. Subsequently, the material was passed 5 more times using the 200 and 100 μm chambers. As the cellulose passes through the chambers, the pressure increases, which favors the interaction between the fibers and the cutting forces, producing cellulose nanofibers [18]. The working solution of CNF was 2.20 μg/ml. CNF was characterized by transmission electron microscopy (TEM) (JEOL, JEM2011, 120 kV) and zeta potential using a nanoparticle analyzer (NanoPartica SZ-100V2, Horiba, Japan). The diameter of the CNF was analyzed by ImageJ software (Fiji distribution, open-source).

2.4. Synthesis and characterization of silver nanoparticles

Silver nanoparticles (AgNPs) were synthesized using a sonochemical method reported previously with some modifications [34]. Chitosan extracted from the shrimp exoskeleton was used as a stabilizing agent. The reduction of silver nitrate into AgNPs was monitored with an UV–Vis spectrophotometer (Shimadzu 1600 UV spectrometer, Kyoto, Japan) from 200 to 800 nm. The AgNPs were characterized by TEM (JEOL, JEM2011), at an acceleration voltage of 120 kV. A 5 μl suspension of AgNPs was placed on carbon-coated copper grids, followed by drying in a desiccator with silica for 16 h. In addition, the hydrodynamic diameter, zeta potential, and polydispersity of the AgNPs were determined by dynamic light scattering (DLS), using a nanoparticle analyzer (NanoPartica SZ-100V2, Horiba, Japan), with a dispersion angle of 173°, at 25 °C. The hydrodynamic diameter, the polydispersity, and zeta potential of AgNPs were 165.6 ± 95.7 nm, 0.383 ± 0.040, and 55.8 ± 5.7 mV, respectively.

2.5. Films preparation

Firstly, 1% (w/v) of chitosan (CHT) solution was prepared by dissolving chitosan powder in an aqueous solution of 1% (v/v) of acetic acid under vigorous stirring for 12 h. Then glycerol was added with continuous stirring at a proportion of 30% (w/w) on a chitosan powder basis. After that, a nanocellulose solution was incorporated in a 10% (v/v) proportion. Subsequently, an AgNPs solution was added at different concentrations (10, 5 and 2.5% v/v). These solutions were left under constant stirring for 1 h. Subsequently, the solutions were sonicated in an ultrasonic bath for 30 min. Finally, the solutions were cast on polyvinyl molds. After casting, the films were dried at 30 °C for 3 days. The coding for film samples is given in Table 1.

Table 1
Film sample codes.

Codes	Description
CHT	Chitosan film
CHT.AgNPs10%	Chitosan film with 10% v/v AgNP
CHT.AgNPs5%	Chitosan film with 5% v/v AgNP
CHT.AgNPs2.5%	Chitosan film with 2.5% v/v AgNP
CHT.CNF	Chitosan film with CNF
CHT.CNF.AgNPs10%	Chitosan film with 10% v/v CNF and 10% v/v of AgNPs
CHT.CNF.AgNPs5%	Chitosan film with 10% v/v CNF and 5% v/v of AgNPs
CHT.CNF.AgNPs2.5%	Chitosan film with 10% v/v CNF and 2,5% v/v of AgNPs

2.6. Films characterization

2.6.1. Fourier transform infrared spectroscopy (FTIR)

FTIR analysis was carried out to determine the main functional groups on the chitosan films. The FTIR spectra were collected at a resolution of 4 cm^{-1} in transmission mode (4000–400 cm^{-1}) using a FTIR spectrophotometer (Alpha, Bruker). The spectra were plotted using Origin Pro 2019 software.

2.6.2. Thermogravimetric analysis (TGA)

The films were analyzed using a TGA-Q500 thermogravimetric analyzer (TA Instruments), equipped with Universal Analysis 2000 software (version 4.5A, TA Instruments). Samples were heated from 30 °C to 800 °C at 10 °C/min under nitrogen. The spectra were plotted using Origin Pro 2019 software.

2.6.3. Scanning electron microscopy (SEM)

The morphology of the films was visualized by SEM (JSM-6390 LV, Jeol), operating at 10 keV, with secondary electrons (SEI) and a spot size of 50. Before the experiment, the samples were coated with a thin film (20 nm) of Gold (Au)-Palladium (Pd), using a high-resolution sputter coater, (208 HR Cressington Company, Watford, UK), coupled to an MTM-20 Cressington High-Resolution Thickness Controller.

2.6.4. Thickness and moisture content and water solubility

Sample thickness was measured using a digital caliper; three different random positions of each film were recorded, and the average thickness was determined. Moisture content (MC) of the samples was determined by measuring the weight loss of film squares (10 mm × 10 mm), before and after drying at 60 °C until constant weight. Water solubility of film samples was determined up to constant weight. Film samples were then cut into strips (1 cm^2) and accurately weighed (M0). They were then placed in 10 mL of distilled water and kept at 25 °C for 24 h. Film samples which had not dissolved were then recovered and dried at 60 °C until constant weight and reweighed (M1). The solubility in water of the films was calculated according to Eq. (1),

$$\text{Solubility } (\%) = \frac{M0 - M1}{M0} x\ 100 \tag{1}$$

Where M0 (g) = is the initial mass of the film sample and M1 (g) = is the mass of the film sample at time t (h).

2.6.5. Light transmission and transparency

The barrier properties of films against ultraviolet (UV) and visible light were investigated by measuring the transmission values at selected wavelength between 300 and 800 nm using a spectrophotometer (UV-2600, Shimadzu, Japan). Film portions of 10 mm × 40 mm were directly placed into the test cell of the spectrophotometer. An empty test cell was used as reference. Absorbance measurement was repeated three times for each sample. The opacity of the films was calculated according to Eq. (2),

$$\text{Opacity} = \frac{Abs600}{d} \tag{2}$$

where Abs_{600} = is the absorbance at 600 nm and d is the film thickness (mm) [35].

2.6.6. Tensile properties

Tensile stress–strain tests were performed at a deformation rate of 50 mm/min in a United SFM-10. Five samples were tested for each film composition according to ASTM D882. In order to determine the tensile strength (TS, MPa), the elastic modulus (EM, MPa) and the elongation at break (EB, %), films were cut into rectangles (150 mm × 10 mm x 0.04 mm) and were mounted between the grips of the machine.

2.6.7. Antimicrobial activity

Antimicrobial activity was assessed using the immersion method. The microorganism assayed was the Gram-negative bacteria *Escherichia coli* (ATCC 25922). Briefly, an inoculum of *E. coli* was prepared in 20.0 mL of NB (Nutrient Broth, Merck) and incubated for a period of 24 h at 37 ± 1 °C. Then, microbial concentrations were adjusted to 1 × 10^8 cells/mL via absorbance at 600 nm. A microbial concentration of 5 × 10^5 cells/mL was obtained using a 200-fold dilution in distilled water. One milliliter of this inoculum was then added to each sample in conical tubes. Samples were incubated for 24 h at 37 °C, under agitation (120 rpm). After this period, the tubes were subjected to vigorous agitation, samples were collected and the number of colony forming units (CFU) was determined by plating serial dilutions. All assays were performed in triplicate and repeated in three independent assays.

The value of antimicrobial activity was calculated according to Eq. (3),

$$\mathrm{R} = \left(log \left(\frac{I}{T} \right) \right) \tag{3}$$

where R = Value of antimicrobial activity, I mean number of viable cells of bacteria in the inoculum after 24 h and T mean number of viable bacteria cells in the antimicrobial test piece after 24 h.

2.7. Statistical analysis

For the analysis of the characterization of cellulose nanofibers and silver nanoparticles, the mean and the standard deviation were used since only the data were described. For the evaluation of properties of the different combinations of chitosan with silver nanoparticles and cellulose nanofibers, the statistical significance was determined to compare means and see the differences in the experimental data for the use of different concentrations with the control. For this, the Student's T test was performed (p value < 0.05) using Origin statistical software, version 9.0.

3. Results and discussion

3.1. Characterization of cellulose nanofibers and silver nanoparticles

It was possible to identify the cellulose nanofibers with an average diameter of 26 ± 6 nm (Fig. 1). It is important to highlight that the dimensions of the CNF obtained in this research are considerably lower than CNF obtained from the thermomechanical pulp of *Pinus radiata*

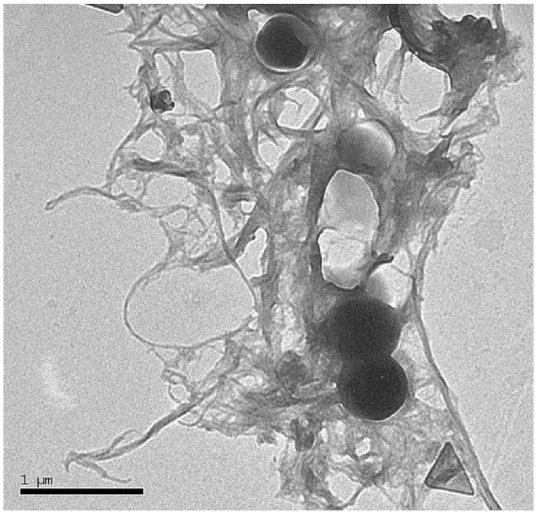

Fig. 1. Transmission electron micrograph of nanocellulose fiber of *Agave tequilana Weber* bagasse.

[36] and for organosolv CNF from *Agave tequilana Weber* bagasse [18]. It was also possible to observe spherical particles between the nanofibers, with an average diameter of 500 nm. These spheres might be lignin particles, which bind to cellulose through complex lignin–carbohydrate bonds, similar to the reported by other authors [36]. Otherwise, the stability of CNF dispersions in aqueous media was measured by zeta potential analysis. The measured zeta potential values of CNF was −26.1 ± 0.56 mV. These values indicated the stability to aggregation [37].

Fig. 2 shows the UV–Vis absorption spectra and the TEM micrograph of AgNPs. It was determined that the AgNPs had a maximum absorbance at 410 nm (Fig. 2A), corresponding to the surface plasmon resonance (SPR), which indicates the formation of AgNPs [38]. Spherical-shaped AgNPs (Fig. 2B), with sizes between 5 and 50 nm were determined. On the other hand, the results of DLS indicated that AgNPs had a mean size of 293.01 ± 8.40, a PDI of 0.393 ± 0.069 and a zeta potential of 44.04 ± 0.87, which indicated the stability of the AgNPs.

3.2. Fourier transform infrared spectroscopy analysis

FTIR analysis was performed to evaluate the structural interaction between chitosan, CNF, and AgNPs. As shown in Fig. 3, the broad absorption peak characteristics of cellulose, the band at 3269 cm^{-1} corresponds to the stretching vibration of O–H and N–H (chitosan), and the peak at 2875 cm^{-1} is attributed to the stretching vibration of C–H. The peak in the range of 3500-3300 cm^{-1} in the CHT.CNF film sample indicates that these polymers interact by intramolecular hydrogen bonding and this contribute to increasing water resistance [39,40]. Another evidence of interaction between CH and CNF is the peak in the range of 2200–2359 cm^{-1} that corresponds to the asymmetric C═N═O stretching vibration, corresponding to the formation of isocyanate group [41]. The band at 1408 cm^{-1} is related to the symmetrical bending vibration of C–H. The band at 1024 cm^{-1} is attributed to the stretching of C–O [4,18,42]. Moreover, the small band observed at 1640 cm^{-1} attributed to the stretching C═C, reported as characteristic of the benzene ring of lignin [18], is associated with the spherical particles observed in CNF by TEM. In addition, the band at 1640 cm^{-1} can also be associated to C═O stretching (amide I) and the band at 1551 cm^{-1} associated to C═O stretching (amide II), while characteristics of chitosan also appeared at 1551 cm^{-1} [4,35,42].

3.3. Thermogravimetric analysis

TGA was performed to evaluate the thermal stability of the samples. Thermograms (TGA) and their first derivatives (DTGA) curves obtained for CHT films with and without AgNPs and CNF are represented in Fig. 3. The DTGA curves of the CNF, chitosan and glycerol (Fig. 4A) show the highest weight loss at 337 °C, 292 °C and 209 °C, respectively. Moreover, all the films show similar curves with three steps of weight loss as a function of temperature. The first step between 30 and 120 °C corresponds to water evaporation [2,3]. Furthermore, there is a second event of weight loss at 125–240 °C, related to glycerol degradation. The last event of weight loss observed at 240–400 °C was due the depolymerization and decomposition of CHT [2,3] and CNF [43]. According to the thermal profiles of the films, it was possible to determine that there were no significant differences in the thermogram curves. This could be related to the presence of AgNPs and CNF in the films, without improving the thermal stability of the films compared to the neat CHT film.

3.4. Morphological analysis

To evaluate the morphology of the CHT, CHT.CNF and CHT.CNF.

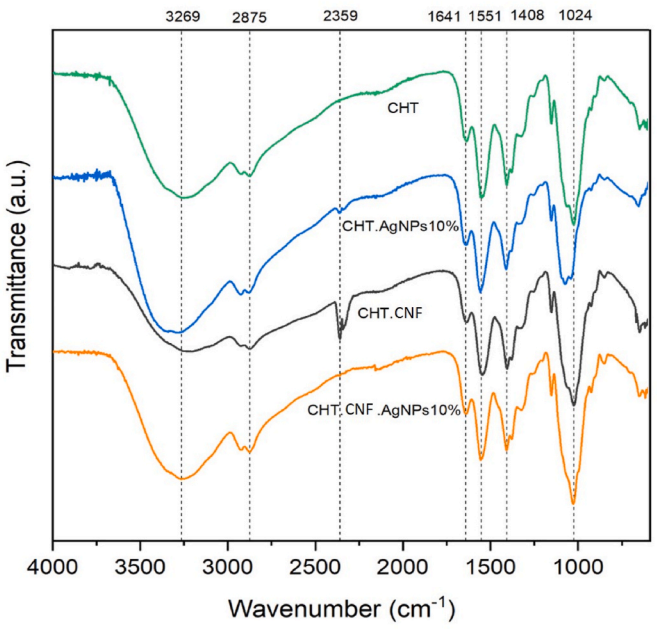

Fig. 3. FTIR spectra of CHT films with CNF and AgNPs.

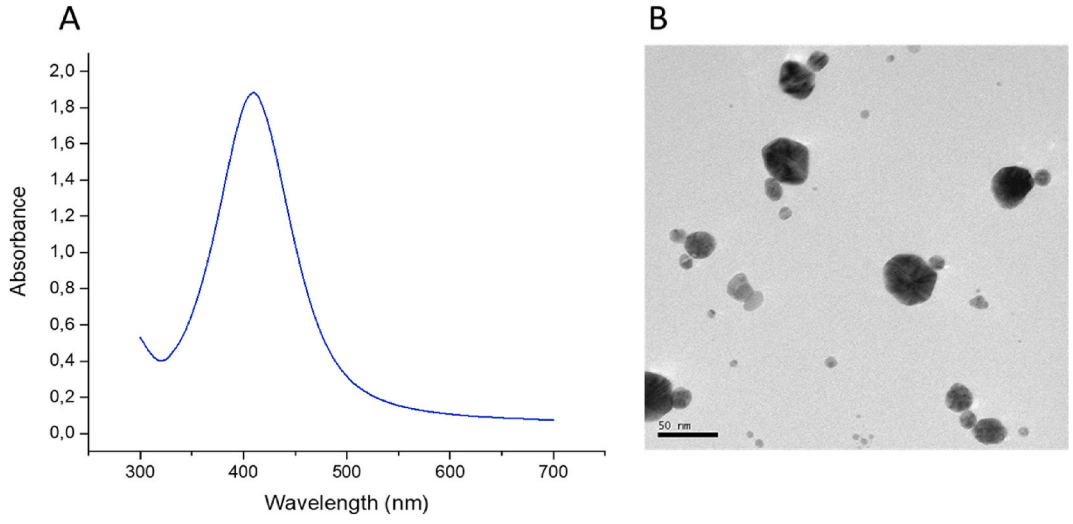

Fig. 2. UV–Vis absorption spectra (A) and transmission electron micrograph (B) of AgNPs.

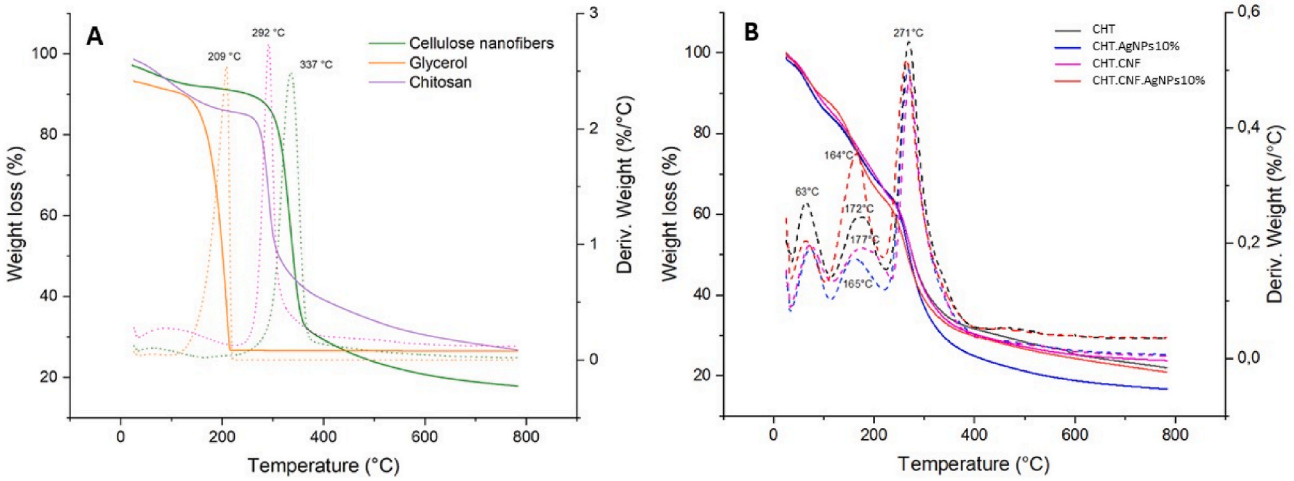

Fig. 4. TGA and DTGA curves of A) CNF, glycerol and CHT, and B) CHT, CHT.AgNPs10%, CHT.CNF, and CHT.CNF.AgNPs10% films. Straight and dotted lines represent the derivative of % weight loss as a function of temperature.

AgNPs films, SEM analysis was performed. Fig. 5 shows the surface images of CHT (Fig. 5a), CHT.AgNPs (Fig. 5b–d) and CHT.CNF.AgNPs (Fig. 5e–h) films. Moreover, Fig. 6 shows the cross-section SEM images of CHT (Fig. 6a), CHT.AgNPs (Fig. 6b–d) and CHT.CNF.AgNPs (Fig. 6e–h) films.

The results determined that the morphology of the surface and cross section of CHT and CHT.AgNPs films are homogeneous and smooth Fig. 6. The CNF incorporation into CHT films led to the appearance of a rougher surface which can be related to accumulation of CNF in the films [3,15]. Moreover, no agglomerations clusters are noticed in the matrix, which could be indicated the CNF was homogeneously distributed mixed into the CHT matrix [3].

3.5. Transparency

The barrier properties of films against UV–visible light were investigated by determining the light transmission of films at wavelengths between 300 and 800 nm (Table 2). The results showed that the presence of CNF or AgNPs raised the opacity value of the CHT film; this being more noticeably in the case of films with AgNPs and CNF. Opacity is a value for the measurement of film transparency. A higher opacity value means lower transparency; however, films can be considered highly transparent when the opacity value is less than 2 [44], such as control chitosan films, 5% and 2.5% AgNP 10% chitosan films, and NFC 10% chitosan films. The CHT and NFC films with 5% and 2.5% content of AGNPs presented opacity values of 4 and 3.49 respectively, these films are more opaque than the pure chitosan films. These results agree with Salari et al., 2018, who found that the incorporation of bacterial cellulose nanocrystals and AgNPs into CHT films, affected the apparent color and reduced the transparency of the films [35]. In the food packaging area, the transparency of the films is a very important factor, since it is related to the choice of consumers; on the other hand, lower transparency can be also a desirable property because the film can act as a UV–Vis light barrier, protecting the food from degradation [3].

Fig. 7 shows the images of the CHT films incorporated with CNF, AgNPs and CNF with AgNPs. Despite the decreasing transparency with the addition of CNF and AgNPs, these films were still clear enough to see through easily (Fig. 7g and h).

3.6. Moisture content and water solubility

Table 3 shows that CHT film had a moisture content of 18.76%; a decrease in the moisture content and water solubility was noticed when 5 and 10% of AgNPs were added to the films [14,35]. This can be related to an increase in the packing of the film network [35]. Moreover, the addition of 10% CNF and AgNPs with CNF also decreased moisture

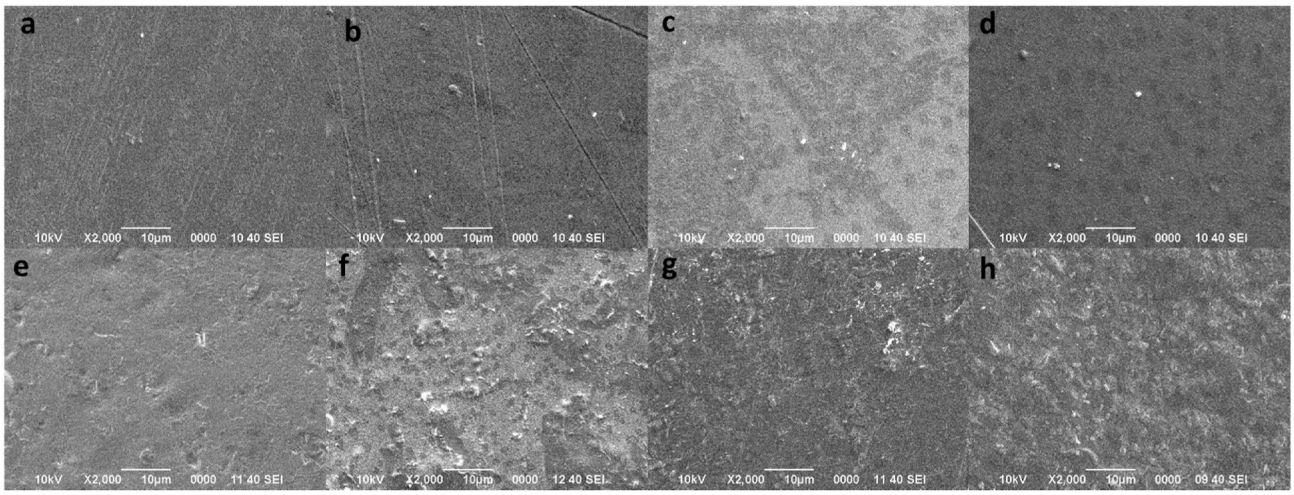

Fig. 5. SEM surface images of (a) CHT, (b) CHT.AgNPs10%, (c) CHT.AgNPs5%, (d) CHT.CNF.AgNPs2.5%, (e) CHT.CNF, (f) CHT.CNF.AgNPs10%, (g) CHT.CNF.AgNPs5%, (h) CHT.CNF.AgNPs2.5%.

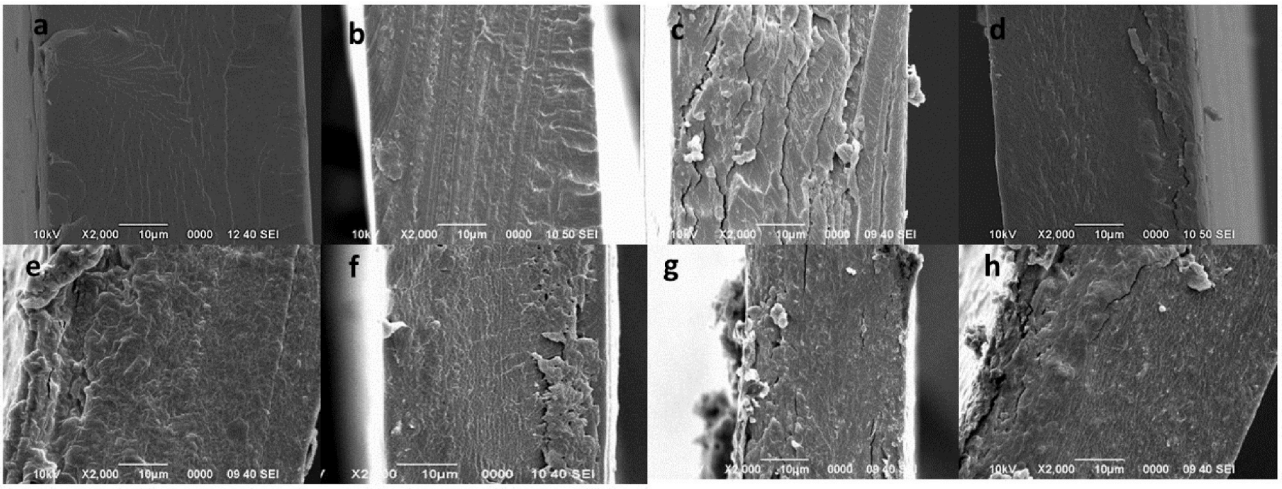

Fig. 6. SEM cross section images of (a) CHT, (b) CHT.AgNPs10%, (c) CHT.AgNPs5%, (d) CHT.CNF.AgNPs2.5%, (e) CHT.CNF, (f) CHT.CNF.AgNPs10%, (g) CHT.CNF.AgNPs5%, (h) CHT.CNF.AgNPs2.5%.

Table 2
Thickness, Light transmission (T%) and opacity values of CHT films incorporated with CNF and AgNPs concentrations (2.5, 5 and 10%).

Treatment	Thickness (mm)	Light transmission (T%)							Opacity value
		300	350	400	500	600	700	800	
CHT	0.052 ± 0.002	51.47 ± 3.85	67.11 ± 3.46	79.49 ± 3.33	86.43 ± 1.74	88.53 ± 1.05	89.24 ± 0.76	89.91 ± 0.47	0.944 ± 0.015
CHT.AgNPs10%	0.045 ± 0.003	59.36 ± 8.34	69.70 ± 7.24	80.14 ± 4.36	86.55 ± 2.21	88.54 ± 1.13	89.54 ± 0.86	90.55 ± 1.20	1.173 ± 0.044
CHT.AgNPs5%	0.043 ± 0.004	68.31 ± 9.40	77.95 ± 4.80	84.25 ± 1.52	88.23 ± 0.21	89.39 ± 0.37	90.27 ± 0.64	90.10 ± 0.81	1.100 ± 0.016
CHT.AgNPs2.5%	0.040 ± 0.005	59.97 ± 3.39	73.33 ± 2.22	82.04 ± 1.11	87.28 ± 0.13	88.96 ± 0.08	89.92 ± 0.45	90.06 ± 0.25	1.710 ± 0.266
CHT.CNF	0.054 ± 0.002	45.25 ± 1.61	57.46 ± 0.78	68.10 ± 1.13	74.51 ± 1.74	77.34 ± 1.87	79.23 ± 1.95	80.66 ± 2.11	1.337 ± 0.103
CHT.CNF.AgNPs10%	0.044 ± 0.005	40.82 ± 6.16	53.25 ± 5.56	61.93 ± 5.37	72.07 ± 2.26	75.73 ± 1.87	78.07 ± 1.88	79.88 ± 1.46	2.041 ± 0.103
CHT.CNF.AgNPs5%	0.040 ± 0.003	20.74 ± 2.07	29.23 ± 2.09	36.84 ± 2.05	45.20 ± 2.25	50.70 ± 2.18	54.95 ± 2.27	58.37 ± 2.15	4.098 ± 0.043
CHT.CNF. AgNPs2.5%	0.050 ± 0.002	25.45 ± 0.90	34.36 ± 1.34	40.95 ± 1.48	49.54 ± 1.60	55.02 ± 1.65	59.23 ± 1.88	62.44 ± 1.85	3.490 ± 0.023

*Values are presented as means ± standard deviation (SD).

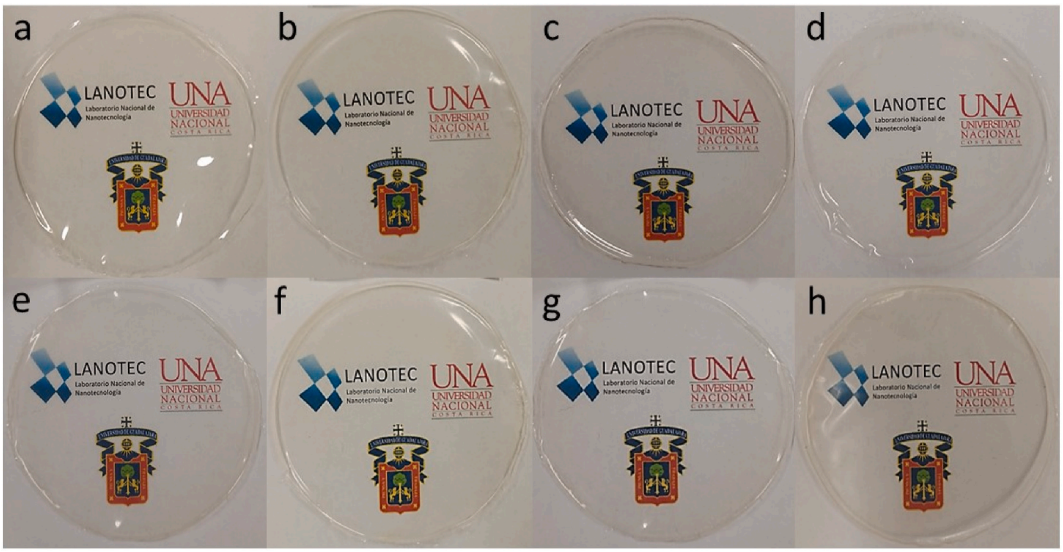

Fig. 7. Imagen of CHT films (a) CHT, (b) CHT.AgNPs10%, (c) CHT.AgNPs5%, (d) CHT.CNF.AgNPs2.5%, (e) CHT.CNF, (f) CHT.CNF.AgNPs10%, (g) CHT.CNF.AgNPs5%, (h) CHT.CNF.AgNPs2.5%.

content and water solubility. This could be attributed to the large specific surface area of CNF and its interaction with CHT chains and AgNPs, which leads to a lower availability of free hydroxyl groups and, consequently, a reduction in hydrophilicity and MC and WS value. This reduction is important for the application of these materials as packaging since the hydrophilic behavior causes a reduced resistance to humidity and this has an influence on the useful life of the packaged foods [44].

Table 3
Moisture content (MC) and water solubility (WS).

Treatment	MC (%)	WS (%)
CHT	18.76 ± 1.93[a]	40.82 ± 1.11[a]
CHT.AgNPs10%	14.79 ± 0.92[b]	35.61 ± 2.90[b]
CHT.AgNPs5%	15.22 ± 5.75[b]	37.34 ± 1.33[b]
CHT.AgNPs2.5%	17.47 ± 2.37[a]	38.48 ± 3.33[a]
CHT.CNF	12.38 ± 0.53[b]	34.92 ± 1.06[b]
CHT.CNF.AgNPs10%	10.91 ± 1.29[b]	34.29 ± 1.86[b]
CHT.CNF.AgNPs5%	11.25 ± 1.23[b]	32.63 ± 2.53[b]
CHT.CNF.AgNPs2.5%	14.56 ± 2.40[b]	30.86 ± 0.36[b]

*Values are presented as means ± standard deviation (SD). values with the same letter do not show significant statistical difference ($p < 0.05$).

3.7. Tensile properties

Chitosan films were subjected to a tensile test where information on the strength, strain at break and modulus were collected, as shown in Fig. 8. An increase in strength and modulus can be seen when the CNF are added to the chitosan film in absence of AgNPs. Once the AgNPs were combined into the film, mechanical propierties decreased overall when AgNPs content increases. An opposite behavior was observed once the AgNPs were in presence of the natural fibers; film properties increased with AgNPs content, reaching to a stiff material at 10% AgNPs. It has been reported that at low AgNPs concentrations, mechanical properties of films remained constant or decreased [7], but recovered to the initial film conditions when using higher concentrations of AgNPs. A synergy between the cellulosic nanofibers and the metallic nanoparticles can be clearly observed from Fig. 8, which means higher interaction between the nanofibers and the chitosan chains, therefore restricting its motion and increasing its rigidity.

3.8. Antimicrobial activity

The antimicrobial activity of different films against *Escherichia coli*, is presented in Table 4. CHT films showed an antibacterial effect, which means that chitosan can partially inhibit their growth. With the incorporation of AgNPs in the films, a total growth inhibition was observed, related to the inherent antimicrobial activity of AgNPs; although a partial inhibition behavior was found only in the treatment with the lowest AgNPs concentration. These results agree with those found in the literature; several papers have reported that chitosan and AgNPs show broad antibacterial activity against Gram-positive and Gram-negative bacteria [2,45]. It has been determined that cationic chitosan can interact with the negatively charged lipopolysaccharides of the cell membrane of microorganisms, then increasing cell permeability, and leading to the leakage of intracellular constituents. Furthermore, chitosan can chelate the environmental ions and nutrients required for bacterial survival, penetrating the cell wall and cell membrane through the cytoplasm and interacting with microbial DNA [3,46,47]. Moreover, silver ions can cause inactivation of the respiratory enzymes leading to the formation of reactive oxygen species resulting in cell damage [48]. Likewise, a total inhibition was also found with the incorporation of CNF in combination with AgNPs in the films. It has been reported the synergistic effect between chitosan and cellulose nanofibers [3,49], which have been attributed to the cell membrane damage caused by the contact of the bacteria with the rigid, narrow, rod-shaped CNF [3]. In addition to their morphology, cellulose nanofibers have a large number of negatively charged hydroxyl groups on their surface that are capable of retaining Ag + nanoparticles and this improves the antibacterial activity of the films and is consistent with studies that have reported that AgNPs are more effective if they are immobilized on a substrate [30].

4. Conclusions

In this work, chitosan and cellulose nanofibers have been successfully prepared from shrimp shells and bagasse agave, respectively. These raw materials are abundant and little-used resources, which contribute to the circular economy by creating new materials. In addition, AgNPs were synthesized by a sonochemical method using CHT as stabilizing agent. CHT films reinforced with CNF and different AgNPs concentrations were produced by casting method. The incorporation of CNF and AgNPs decreases the transparency of the films, moisture content and water solubility but increase the opacity. This is important, since one of the drawbacks of using chitosan films as food packaging is its high solubility in water. In addition, increasing the opacity limits the transmission of UV and visible light and this reduces the oxidative deterioration of food. Moreover, the incorporation of CNF.AgNPs5% and AgNPs2.5% into the CHT films increased the mechanical properties and displayed a total antibacterial activity against E.coli compared to the neat CHT-based films. This work highlights the great potential of CHT films reinforced with CNF and AgNPs to act as green alternative for food packaging.

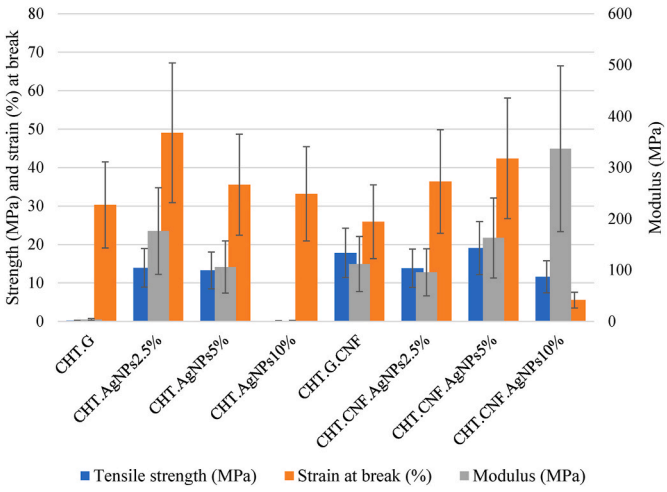

Fig. 8. Tensile properties of the chitosan films.

Table 4
Antimicrobial activity of chitosan films with CNF and different AgNPs concentrations (2.5, 5, and 10% v/v).

Treatment	Antimicrobial activity (R)
CHT	5.45 ± 0.08
CHT.AgNPs10%	Total
CHT.AgNPs5%	Total
CHT.AgNPs2.5%	7.49 ± 0.06
CHT.CNF	6.44 ± 0.08
CHT.CNF.AgNPs10%	Total
CHT.CNF.AgNPs5%	Total
CHT.CNF.AgNPs2.5%	Total

*Values are presented as means ± standard deviation (SD).

Declaration of competing interest

The authors declare that they have no known competing financial interests or personal relationships that could have appeared to influence the work reported in this paper.

Data availability

No data was used for the research described in the article.

Acknowledgments

G.M.V wants to acknowledge the financial support from a Red

NANOCELIA-CYTED scholarship. This research received financial support from the National Council of State Universities of Costa Rica (Special Fund for Higher Education). Authors greatly appreciate the TEM support from Mr. Reinaldo Pereira at LANOTEC.

References

[1] P. Cazón, M.J. Vázquez, Mechanical and barrier properties of chitosan combined with other components as food packaging film, Environ. Chem. Lett. 18 (2020) 257–267, https://doi.org/10.1007/s10311-019-00936-3.

[2] G.O. Akalin, O. Oztuna Taner, T. Taner, The preparation, characterization and antibacterial properties of chitosan/pectin silver nanoparticle films, Polym. Bull. 79 (2021) 3495–3512, https://doi.org/10.1007/s00289-021-03667-0.

[3] A.S. Ribeiro, S.M. Costa, D.P. Ferreira, R.C. Calhelha, L. Barros, D. Stojković, M. Soković, I.C. Ferreira, R. Fangueiro, Chitosan/nanocellulose electrospun fibers with enhanced antibacterial and antifungal activity for wound dressing applications, React. Funct. Polym. 159 (2021), 104808, https://doi.org/10.1016/j.reactfunctpolym.2020.104808.

[4] H. Talebi, F.A. Ghasemi, A. Ashori, The effect of nanocellulose on mechanical and physical properties of chitosan-based biocomposites, J. Elastomers Plast. 54 (2022) 22–41, https://doi.org/10.1177/00952443211017169.

[5] K.W. Choo, R. Dhital, L. Mao, M. Lin, A.J.F.P. Mustapha, S. Life, Development of polyvinyl alcohol/chitosan/modified bacterial nanocellulose films incorporated with 4-hexylresorcinol for food packaging applications, Food Packag. Shelf Life 30 (2021), 100769, https://doi.org/10.1016/j.fpsl.2021.100769.

[6] G. Amor, M. Sabbah, L. Caputo, M. Idbella, V. De Feo, R. Porta, T. Fechtali, G. Mauriello, Basil essential oil: composition, antimicrobial properties, and microencapsulation to produce active chitosan films for food packaging, Foods 10 (2021) 1–16, https://doi.org/10.3390/foods10010121.

[7] N. Mohamed, N.G. Madian, Evaluation of the mechanical, physical and antimicrobial properties of chitosan thin films doped with greenly synthesized silver nanoparticles, Mater. Today Commun. 25 (2020), 101372, https://doi.org/10.1016/j.mtcomm.2020.101372.

[8] J. Pires, C.D.d. Paula, V.G.L. Souza, A.L. Fernando, I.J. Coelhoso, Understanding the barrier and mechanical behavior of different nanofillers in chitosan films for food packaging, Polymers 13 (2021) 721, https://doi.org/10.3390/polym13050721.

[9] R. Priyadarshi, J.-W. Rhim, Chitosan-based biodegradable functional films for food packaging applications, Innovat. Food Sci. Emerg. Technol. 62 (2020), 102346, https://doi.org/10.1016/j.ifset.2020.102346.

[10] K. Kusmono, M.W. Wildan, F.I. Lubis, Fabrication and characterization of chitosan/cellulose nanocrystal/glycerol bio-composite films, Polymers 13 (2021) 1096, https://doi.org/10.3390/polym13071096.

[11] Y. Peng, H. Zhou, Y. Wu, Z. Ma, R. Zhang, H. Tu, L. Jiang, A new strategy to construct cellulose-chitosan films supporting Ag/Ag2O/ZnO heterostructures for high photocatalytic and antibacterial performance, J. Colloid Interface Sci. 609 (2022) 188–199, https://doi.org/10.1016/j.jcis.2021.11.155.

[12] Y. Liu, Y. Yuan, S. Duan, C. Li, B. Hu, A. Liu, D. Wu, H. Cui, L. Lin, J. He, Preparation and characterization of chitosan films with three kinds of molecular weight for food packaging, Int. J. Biol. Macromol. 155 (2020) 249–259, https://doi.org/10.1016/j.ijbiomac.2020.03.217.

[13] S. Ramesh, P. Radhakrishnan, Cellulose nanoparticles from agro-industrial waste for the development of active packaging, Appl. Surf. Sci. 484 (2019) 1274–1281, https://doi.org/10.1016/j.apsusc.2019.04.003.

[14] W. Zhang, W. Jiang, Antioxidant and antibacterial chitosan film with tea polyphenols-mediated green synthesis silver nanoparticle via a novel one-pot method, Int. J. Biol. Macromol. 155 (2020) 1252–1261, https://doi.org/10.1016/j.ijbiomac.2019.11.093.

[15] S.M. Mohammadi Sadati, N. Shahgholian-Ghahfarrokhi, E. Shahrousvand, J. Mohammadi-Rovshandeh, M. Shahrousvand, Edible chitosan/cellulose nanofiber nanocomposite films for potential use as food packaging, Mater. Technol. 37 (2022) 1276–1288, https://doi.org/10.1080/10667857.2021.1934367.

[16] S. Jancy, R. Shruthy, R. Preetha, Fabrication of packaging film reinforced with cellulose nanoparticles synthesised from jack fruit non-edible part using response surface methodology, Int. J. Biol. Macromol. 142 (2020) 63–72, https://doi.org/10.1016/j.ijbiomac.2019.09.066.

[17] S. Ventura-Cruz, A. Tecante, Nanocellulose and microcrystalline cellulose from agricultural waste: review on isolation and application as reinforcement in polymeric matrices, Food Hydrocolloids 118 (2021), 106771, https://doi.org/10.1016/j.foodhyd.2021.106771.

[18] H. Palacios Hinestroza, J.A. Hernández Diaz, M. Esquivel Alfaro, G. Toriz, O. J. Rojas, B.C.J. Sulbarán-Rangel, Engineering, Isolation and characterization of nanofibrillar cellulose from Agave tequilana Weber bagasse, Adv. Mater. Sci. 2019 (2019), https://doi.org/10.1155/2019/1342547.

[19] M.A. Gallardo-Sánchez, T. Diaz-Vidal, A.B. Navarro-Hermosillo, E.B. Figueroa-Ochoa, R. Ramirez Casillas, J. Anzaldo Hernández, L.C. Rosales-Rivera, J.F. A. Soltero Martínez, S. García Enríquez, E.R. Macías-Balleza, Optimization of the obtaining of cellulose nanocrystals from agave Tequilana weber var. Azul Bagasse by acid hydrolysis, Nanomaterials 11 (2021) 520, https://doi.org/10.3390/nano11020520.

[20] J.A. Hernández, V.H. Romero, A. Escalante, G. Toriz, O.J. Rojas, B. Sulbarán-Rangel, Agave tequilana bagasse as source of cellulose nanocrystals via organosolv treatment, Bioresources 13 (2018) 3604–3614, https://doi.org/10.15376/biores.13.2.3603-3614.

[21] M.G. Lomelí-Ramírez, E.M. Valdez-Fausto, M. Rentería-Urquiza, R.M. Jiménez-Amezcua, J. Anzaldo Hernández, J.G. Torres-Rendon, S. García Enriquez, Study of green nanocomposites based on corn starch and cellulose nanofibrils from Agave tequilana Weber, Carbohydr. Polym. 201 (2018) 9–19, https://doi.org/10.1016/j.carbpol.2018.08.045.

[22] X. Chang, Y. Hou, Q. Liu, Z. Hu, Q. Xie, Y. Shan, G. Li, S.J. Ding, Physicochemical and antimicrobial properties of chitosan composite films incorporated with glycerol monolaurate and nano-TiO2, Food Hydrocolloids 119 (2021), 106846, https://doi.org/10.1016/j.foodhyd.2021.106846.

[23] Z. Liu, M. Du, H. Liu, K. Zhang, X. Xu, K. Liu, J. Tu, Q. Liu, Chitosan films incorporating litchi peel extract and titanium dioxide nanoparticles and their application as coatings on watercored apples, Prog. Org. Coating 151 (2021), 106103, https://doi.org/10.1016/j.porgcoat.2020.106103.

[24] V.G.L. Souza, M.M. Alves, C.F. Santos, I.A. Ribeiro, C. Rodrigues, I. Coelhoso, A. L. Fernando, Biodegradable chitosan films with ZnO nanoparticles synthesized using food industry by-products—production and characterization, Coatings 11 (2021) 646, https://doi.org/10.3390/coatings11060646.

[25] V. Bui, D. Park, Y.-C. Lee, Chitosan combined with ZnO, TiO2 and Ag nanoparticles for antimicrobial wound healing applications: a mini review of the research trends, Polymers 9 (2017) 21, https://doi.org/10.3390/polym9010021.

[26] A.A. Wardana, P. Kingwascharapong, F. Tanaka, F. Tanaka, CuO nanoparticles/Indonesian cedarwood essential oil-loaded chitosan coating film: characterisation and antifungal improvement against Penicillium spp, Int. J. Food Sci. Technol. 56 (2021) 4224–4238, https://doi.org/10.1111/ijfs.15195.

[27] H. Zhao, L. Zhang, S. Zheng, S. Chai, J. Wei, L. Zhong, Y. He, J. Xue, Bacteriostatic activity and cytotoxicity of bacterial cellulose-chitosan film loaded with in-situ synthesized silver nanoparticles, Carbohydr. Polym. 281 (2022), 119017, https://doi.org/10.1016/j.carbpol.2021.119017.

[28] S.K. Bajpai, S. Ahuja, N. Chand, M. Bajpai, Nano cellulose dispersed chitosan film with Ag NPs/Curcumin: an in vivo study on Albino Rats for wound dressing, Int. J. Biol. Macromol. 104 (2017) 1012–1019, https://doi.org/10.1016/j.ijbiomac.2017.06.096.

[29] S. Ediyilyam, B. George, S.S. Shankar, T.T. Dennis, S. Wacławek, M. Černík, V. Padil, Chitosan/gelatin/silver nanoparticles composites films for biodegradable food packaging applications, Polymers 13 (2021) 1680, https://doi.org/10.3390/polym13111680.

[30] X. Dai, S. Li, S. Li, K. Ke, J. Pang, C. Wu, Z. Yan, High antibacterial activity of chitosan films with covalent organic frameworks immobilized silver nanoparticles, Int. J. Biol. Macromol. 202 (2022) 407–417, https://doi.org/10.1016/j.ijbiomac.2021.12.174.

[31] M.R. Kasaai, J. Arul, G. Charlet, Intrinsic viscosity–molecular weight relationship for chitosan, J. Polym. Sci. B Polym. Phys. 38 (2000) 2591–2598, https://doi.org/10.1002/1099-0488(20001001)38:19<2591::AID-POLB110>3.0.CO;2-6.

[32] R. Czechowska-Biskup, D. Jarosińska, B. Rokita, P. Ulański, J.M.J. Rosiak, A. o Chitin, i. Derivatives, Determination of degree of deacetylation of chitosan-comparision of methods, Prog. Chem. Appl.Chitin Derivat. 17 (2012) 5–20.

[33] E.M. Santos Ventura, Escalante Álvarez, M.A. Gutiérrez, A. B, B. Sulbarán-Rangel, Unbleached cellulose from waste corncob for isolation of cellulose nanocrystals, Emerg. Mater. Res. 9 (2020) 1258–1265, https://doi.org/10.1680/jemmr.20.00073.

[34] R. Alvarado Meza, F. Solera, J. Vega-Baudrit, Síntesis sonoquímica de nanopartículas de óxido de cinc y de plata estabilizadas con quitosano. Evaluación de su actividad antimicrobiana, Revista Iberoamericana de Polímeros. 15 (2014).

[35] M. Salari, M.S. Khiabani, R.R. Mokarram, B. Ghanbarzadeh, H.S. Kafil, Development and evaluation of chitosan based active nanocomposite films containing bacterial cellulose nanocrystals and silver nanoparticles, Food Hydrocolloids 84 (2018) 414–423, https://doi.org/10.1016/j.foodhyd.2018.05.037.

[36] J. Vergara-Figueroa, O. Erazo, H. Pesenti, P. Valenzuela, A. Fernández-Pérez, W. Gacitúa, Development of thin films from thermomechanical pulp nanofibers of radiata pine (Pinus radiata D. Don) for applications in bio-based nanocomposites, Fibers 11 (2022) 1, https://doi.org/10.3390/fib11010001.

[37] B. Çiçek Özkan, M.J.C. Güner, Isolation, characterization, and comparison of nanocrystalline cellulose from solid wastes of horse chestnut and chestnut seed shell, Cellulose 29 (2022) 6629–6644, https://doi.org/10.1007/s10570-022-04682-8.

[38] L.A. Laime-Oviedo, A.A. Soncco-Ccahui, G. Peralta-Alarcon, C.A. Arenas-Chávez, J. L. Pineda-Tapia, J.C. Díaz-Rosado, A. Alvarez-Risco, S. Del-Aguila-Arcentales, N. M. Davies, J. Yáñez, Optimization of synthesis of silver nanoparticles conjugated with lepechinia meyenii (salvia) using plackett-burman design and response surface methodology—preliminary antibacterial activity, Processes 10 (2022) 1727, https://doi.org/10.3390/pr10091727.

[39] Z. Deng, J. Jung, Y. Zhao, Development, characterization, and validation of chitosan adsorbed cellulose nanofiber (CNF) films as water resistant and antibacterial food contact packaging, LWT - Food Sci. Technol. (Lebensmittel-Wissenschaft -Technol.) 83 (2017) 132–140, https://doi.org/10.1016/j.lwt.2017.05.013.

[40] A. Khan, R.A. Khan, S. Salmieri, C. Le Tien, B. Riedl, J. Bouchard, G. Chauve, V. Tan, M.R. Kamal, M. Lacroix, Mechanical and barrier properties of nanocrystalline cellulose reinforced chitosan based nanocomposite films, Carbohydr. Polym. 90 (2012) 1601–1608, https://doi.org/10.1016/j.carbpol.2012.07.037.

[41] Merk. IR Spectrum Table & Chart. (accessed on 21 August 2023). Available from: https://www.sigmaaldrich.com/BS/en/technical-documents/technical-article/analytical-chemistry/photometry-and-reflectometry/ir-spectrum-table.
[42] H. Zeng, H. Hao, X. Wang, Z. Shao, Chitosan-based composite film adsorbents reinforced with nanocellulose for removal of Cu(II) ion from wastewater: preparation, characterization, and adsorption mechanism, Int. J. Biol. Macromol. 213 (2022) 369–380, https://doi.org/10.1016/j.ijbiomac.2022.05.103.
[43] P.A.Z. Hasibuan, M. Tanjung, S. Gea, K.M. Pasaribu, M. Harahap, Y.A. Perangin-Angin, A. Prayoga, J.G. Ginting, Antimicrobial and antihemolytic properties of a CNF/AgNP-chitosan film: a potential wound dressing material, Heliyon 7 (2021), e08197, https://doi.org/10.1016/j.heliyon.2021.e08197.
[44] H. Haghighi, M. Gullo, S. La China, F. Pfeifer, H.W. Siesler, F. Licciardello, A. Pulvirenti, Characterization of bio-nanocomposite films based on gelatin/polyvinyl alcohol blend reinforced with bacterial cellulose nanowhiskers for food packaging applications, Food Hydrocolloids 113 (2021), 106454, https://doi.org/10.1016/j.foodhyd.2020.106454.
[45] W.G. Sganzerla, L.E.N. Castro, C.G. da Rosa, A.d.R. Almeida, F.W. Maciel-Silva, P. R.G. Kempe, A.L.R. de Oliveira, T. Forster-Carneiro, F.C. Bertoldi, P.L.M. Barreto, A.P.d.L. Veeck, M.R. Nunes, Production of nanocomposite films functionalized with silver nanoparticles bioreduced with rosemary (Rosmarinus officinalis L.) essential oil, J. Agric. Food Res. 11 (2023), 100479, https://doi.org/10.1016/j.jafr.2022.100479.
[46] P. Sahariah, M. Másson, Antimicrobial chitosan and chitosan derivatives: a review of the structure–activity relationship, Biomacromolecules 18 (2017) 3846–3868, https://doi.org/10.1021/acs.biomac.7b01058.
[47] C.-L. Ke, F.-S. Deng, C.-Y. Chuang, C.-H. Lin, Antimicrobial actions and applications of chitosan, Polymers 13 (2021) 904, https://doi.org/10.3390/polym13060904.
[48] M. Majeed, K.R. Hakeem, R.U.J. Rehman, Synergistic effect of plant extract coupled silver nanoparticles in various therapeutic applications-present insights and bottlenecks, Chemosphere 288 (2022), 132527, https://doi.org/10.1016/j.chemosphere.2021.132527.
[49] J. Jacob, G. Peter, S. Thomas, J.T. Haponiuk, S. Gopi, Chitosan and polyvinyl alcohol nanocomposites with cellulose nanofibers from ginger rhizomes and its antimicrobial activities, Int. J. Biol. Macromol. 129 (2019) 370–376, https://doi.org/10.1016/j.ijbiomac.2019.02.052.